Available online at www.sciencedirect.com
ScienceDirect
Journal of Sound and Vibration 320 (2009) 60–83
JOURNAL OF SOUND AND VIBRATION
www.elsevier.com/locate/jsvi

Error analysis and feasibility study of dynamic stiffness matrix-based damping matrix identification

Gokhan O. Ozgen, Jay H. Kim*

Structural Dynamics Research Lab, Mechanical, Industrial and Nuclear Engineering Department, University of Cincinnati, Cincinnati, OH 45221-0072, USA

Received 21 December 2006; received in revised form 21 July 2008; accepted 21 July 2008
Handling Editor: S. Bolton
Available online 6 September 2008

Abstract

Developing a method to formulate a damping matrix that represents the actual spatial distribution and mechanism of damping of the dynamic system has been an elusive goal. The dynamic stiffness matrix (DSM)-based damping identification method proposed by Lee and Kim is attractive and promising because it identifies the damping matrix from the measured DSM without relying on any unfounded assumptions. However, in ensuing works it was found that damping matrices identified from the method had unexpected forms and showed traces of large variance errors. The causes and possible remedies of the problem are sought for in this work. The variance and leakage errors are identified as the major sources of the problem, which are then related to system parameters through numerical and experimental simulations. An improved experimental procedure is developed to reduce the effect of these errors in order to make the DSM-based damping identification method a practical option.

1. Introduction

Often the damping matrix is formulated by using an extremely simple model such as the viscous, structural, or proportional damping model when the equation of motion of a dynamic system is formulated. Such simple models were introduced mainly for mathematical convenience, and match only the overall energy loss effect, ignoring the actual mechanism and spatial distribution of the damping in the system. Motivated by a desire to formulate the damping matrix that correctly describes both the mechanism and spatial distribution of damping, various approaches have been proposed. Many of these approaches use experimentally identified modal parameters, frequencies, damping ratios and mode shape vectors, to find the damping matrix [1–11]. This requires modal parameters to be found first, which are then used to find the damping matrix. Because the damping property has physically much smaller signature than the stiffness and inertia properties, the process amplifies experimental errors involved with the prior step to ruin the damping matrix to be found.

*Corresponding author. Tel.: +1 513 556 6300.
E-mail address: jay.kim@uc.edu (J.H. Kim).

0022-460X/$ - see front matter © 2008 Elsevier Ltd. All rights reserved.
doi:10.1016/j.jsv.2008.07.021

Nomenclature

c	viscous damping coefficient
$\mathbf{C}$	viscous damping matrix
$\mathbf{C}_{\text{exp}}$	experimental viscous damping matrix
dof	degree of freedom
$\mathbf{D}$	structural damping matrix
DFT	discrete Fourier transform
DSM	dynamic stiffness matrix
f	frequency (Hz)
FEA	finite element analysis
FFT	fast Fourier transform
FRF	frequency response function
$\mathbf{H}(\omega)$	FRF matrix
$\mathbf{H}_{\text{exp}}(\omega)$	experimental FRF matrix
i	mode number
$\mathbf{I}$	identity matrix
IFFT	inverse fast Fourier transform
j	complex term $(=\sqrt{-1})$
k	number of frequency points/stiffness
k_i	stiffness of ith element
$\mathbf{K}$	stiffness matrix
$\mathbf{K}_{\text{exp}}$	experimental stiffness matrix
$\mathbf{L}(\omega)$	generalized damping matrix
m	mass
m_i	mass of ith element
M	number of measurement points/modal mass
$\mathbf{M}$	mass matrix
$\mathbf{M}_{\text{exp}}$	experimental mass matrix
MRIT	multi-reference impact testing
MIMO	multi-input–multi-output
Q_r	modal scaling factor for rth mode
r	mode number
$\mathbf{S}_D(\omega)$	dynamic stiffness matrix of analytical model
$\mathbf{S}_{D_{\text{exp}}}(\omega)$	experimental dynamic stiffness matrix
SIMO	single input–multi-output
SVD	singular value decomposition
T	sampling period
$\mathbf{U}(\omega)$	left-hand side matrix
$\mathbf{V}(\omega)$	right-hand side matrix
Δf	frequency increment (Hz)
$\mathbf{\Sigma}(\omega)$	singular value matrix
α	proportionality constant
λ_r	complex modal frequency for rth mode
ξ	damping ratio
ω	circular frequency (rad/s)
$\boldsymbol{\psi}$	modal matrix
$\boldsymbol{\psi}_r$	modal vector for rth mode
$\mathbf{\Omega}_i$	undamped modal frequency of the ith mode (rad/s)

Some approaches were developed to formulate damping matrices directly from measured frequency response functions (FRFs), which eliminated the need to rely on modal parameters [12–17]. Among them, the procedure developed by Lee and Kim [17] obtained the damping matrix from the dynamic stiffness matrix (DSM) by inverting the measured frequency response function matrix (FRM). The method developed by Lee and Kim [17] can be summarized by three steps.

In the first step, measured FRFs are put into a matrix form as follows:

$$\mathbf{H}_{\text{exp}}(\omega)=\begin{bmatrix} H_{11}(\omega) & \cdots & H_{1M}(\omega) \\ \vdots & \ddots & \vdots \\ H_{M1}(\omega) & \cdots & H_{MM}(\omega) \end{bmatrix}, \tag{1}$$

where $\mathbf{H}_{\text{exp}}(\omega)$ is the measured FRF matrix, ω is the circular frequency (rad/s) and M is the measurement degrees of freedom (dofs). In the second step, dynamic stiffness matrix of the experimental model $\mathbf{S}_{D\,\text{exp}}(\omega)$ is obtained by inverting $\mathbf{H}_{\text{exp}}(\omega)$:

$$\mathbf{S}_{D\,\text{exp}}(\omega)=\mathbf{H}_{\text{exp}}(\omega)^{-1}. \tag{2}$$

The final step utilizes the fact that the imaginary part of the dynamic stiffness matrix, $\mathbf{S}_{D\,\text{exp}}(\omega)$, represents the energy loss property. That is, $\mathbf{S}_{D\,\text{exp}}(\omega)=\mathbf{K}_{\text{exp}}-\omega^2\mathbf{M}_{\text{exp}}+\text{j}\mathbf{L}_{\text{exp}}(\omega)$, where $\mathbf{M}_{\text{exp}}$ and $\mathbf{K}_{\text{exp}}$ are the mass and stiffness matrices, $\text{j}=\sqrt{-1}$, and $\mathbf{L}_{\text{exp}}(\omega)$ is a real valued generalized damping matrix. The subscript exp indicates an experimentally obtained term. Obviously, $\mathbf{L}_{\text{exp}}(\omega)$ can be obtained as

$$\mathbf{L}_{\text{exp}}(\omega)=\text{Imag}\big(\mathbf{S}_{D_{\text{exp}}}(\omega)\big). \tag{3a}$$

Mass and stiffness matrices are related with the dynamic stiffness matrix as follows:

$$-\mathbf{M}_{\exp}\omega^2 + \mathbf{K}_{\exp} = \mathrm{Re}\big(\mathbf{S}_{D\,\exp}(\omega)\big). \tag{3b}$$

At a given frequency, the magnitudes of the elements of $\mathbf{L}_{\exp}(\omega)$ represent the form of the spatial distribution of damping. The frequency function that defines each element of $\mathbf{L}_{\exp}(\omega)$ represents the damping mechanism of the system at the corresponding nodal point.

While the approach is very attractive because of its simplicity, practical difficulties have been encountered in follow-on studies by Hylok [18] and Ozgen and Kim [19]. Hylok's experimental work [18] showed the identified damping matrix was highly susceptible to measurement errors, which was confirmed by Ozgen and Kim [19]. The major objectives of this paper are to identify the causes of these measurement errors and quantify them, and to develop an improved experimental procedure to enable obtaining a more accurate damping matrix.

2. Effects of measurement errors

2.1. Previous experimental work

Fig. 1 shows the test object, an aluminum beam suspended by bungee cords to simulate a free–free beam that was used by Hylok [18] to implement the dynamic stiffness matrix-based damping matrix identification. A 6×6 FRF matrix was obtained using single-axis accelerometers installed at 6 points along the longitudinal center-line of the beam. The multi-reference impact testing (MRIT) [20] was used.

Measured FRFs are shown in Fig. 2, which form a spatial plot of the magnitudes of FRFs. The real part, $-\mathbf{M}_{\exp}\omega^2 + \mathbf{K}_{\exp}$, and imaginary part, $\mathbf{L}_{\exp}(\omega)$, of the dynamic stiffness matrix obtained by inverting the experimental FRF matrix are shown in Figs. 3 and 4 respectively. The imaginary part of the dynamic stiffness matrix in Fig. 4 is the spatial plot of the damping effect.

Compared to the FRFs shown in Fig. 2, the elements of the dynamic stiffness matrix in Figs. 3 and 4 show much more scattered patterns, which indicates that measurement errors influence dynamic stiffness matrix much more than FRFs. It can also be seen from the comparison of Figs. 3 and 4, especially in diagonal elements, that the imaginary part is more scattered than the real part. This can be explained by the fact that the imaginary part that represents the damping effect has much smaller signal to noise (S/N) ratio because its magnitude is much smaller than that of the real part that represents the mass and stiffness effect.

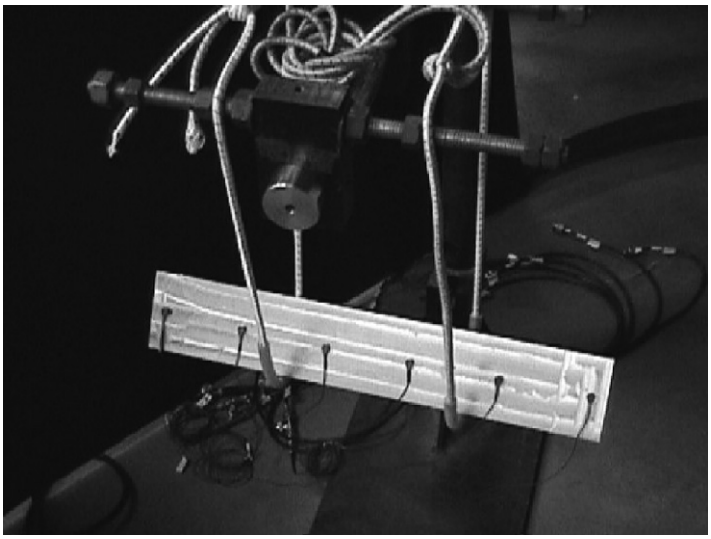

Fig. 1. Experimental setup, suspended aluminum beam used in Ref. [18].

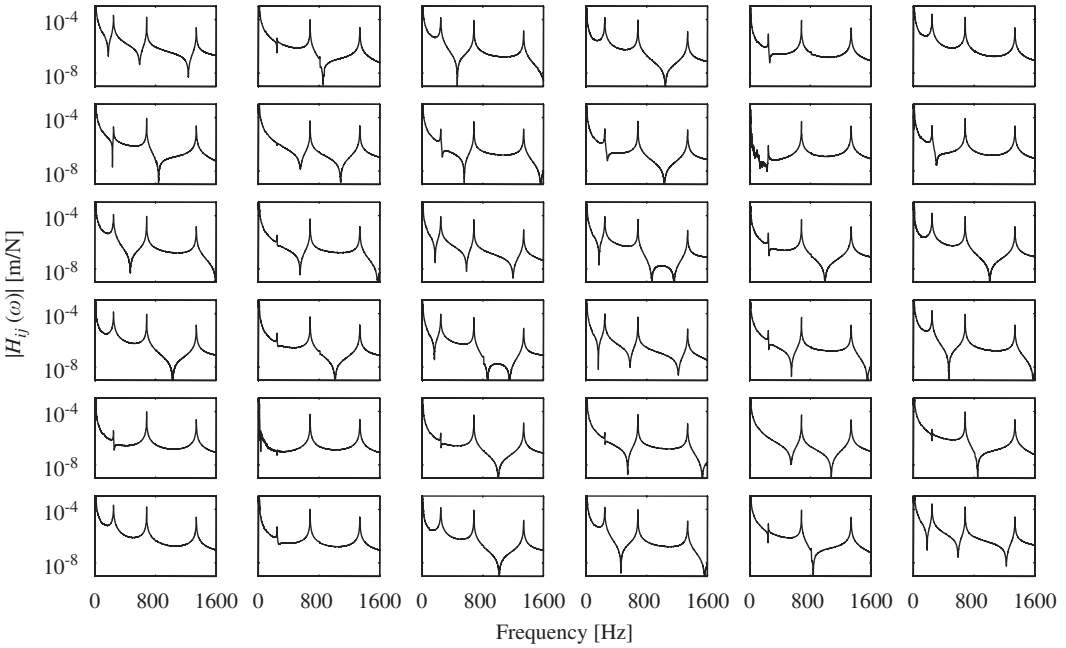

Fig. 2. Spatial plot of the experimental FRF matrix of Hylok's aluminum beam used in Ref. [18].

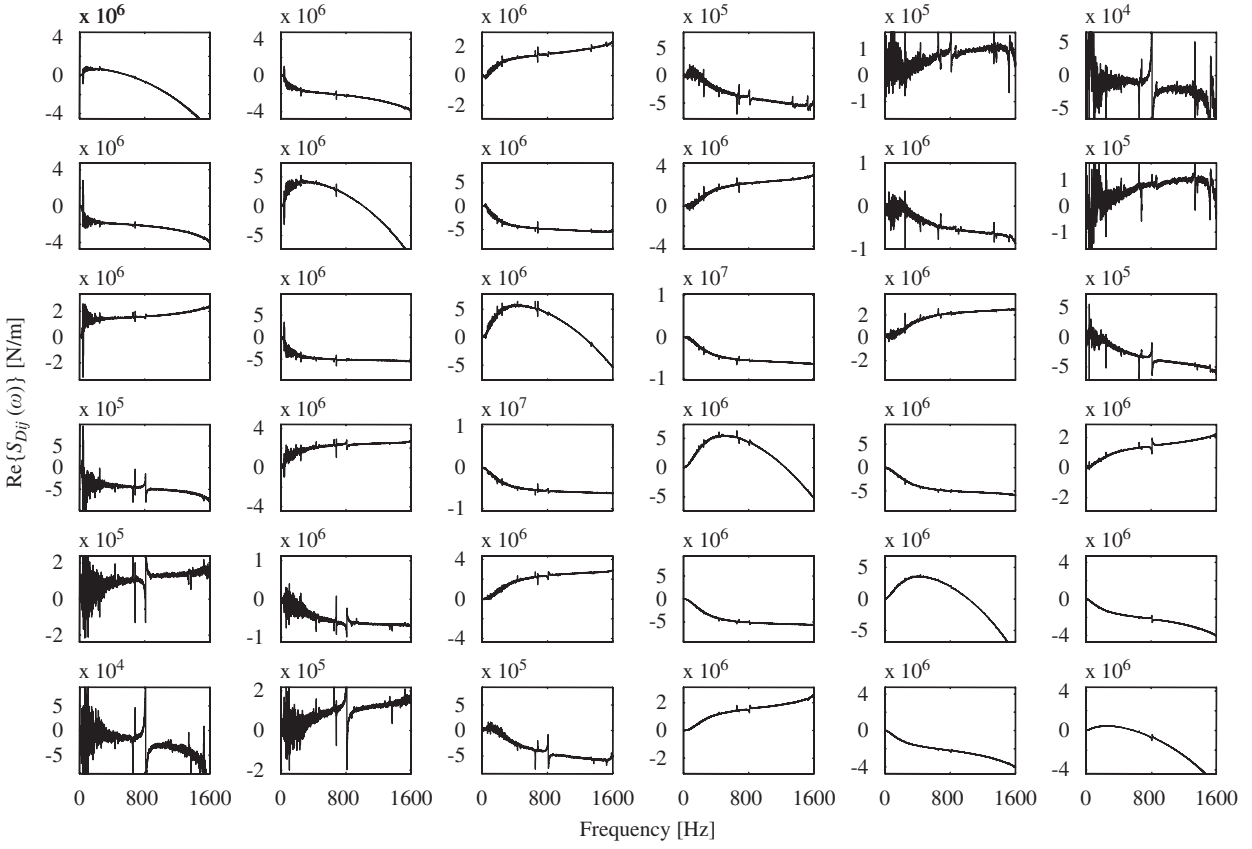

Fig. 3. Spatial plot of the real part of the experimental dynamic stiffness matrix of Hylok's aluminum beam used in Ref. [18].

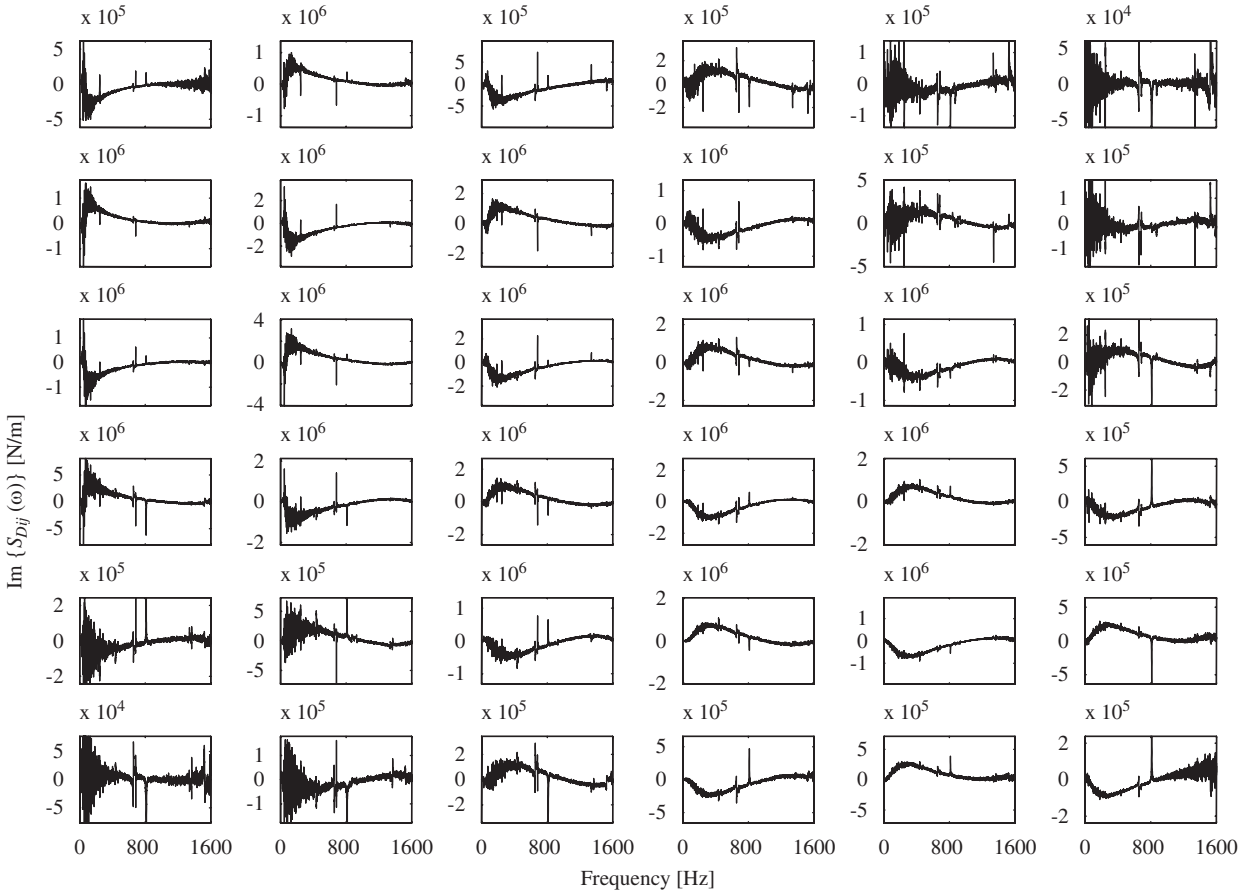

Fig. 4. Spatial plot of the imaginary part of the experimental dynamic stiffness matrix of Hylok's aluminum beam used in Ref. [18].

Fig. 4 shows that all diagonal elements of the damping matrix $\mathbf{L}_{\text{exp}}(\omega)$ are negative valued in a wide frequency range. This indicates that the damping mechanism creates energy rather than dissipating, which is obviously not possible, therefore must be a result of a measurement error. The variance error does not explain this phenomenon, which leads to the hypothesis that the identified damping matrix must be influenced by a bias type error.

In general, bias errors in FRF measurements are associated with the alias effect, system nonlinearity, external disturbances (e.g., unmeasured forces) and the leakage error [21]. The alias error is a less likely source because the data was acquired using an anti-aliasing filter. Nonlinearity is also not a possibility either because of the simplicity of the test structure and low level of the excitation. Therefore, the leakage is considered a more likely source of the bias error.

The exponential window was not used to reduce the leakage error in Hylok's work [18], which used the impact testing because it would have introduced artificial damping effects [22], thus would have ruined the purpose of testing, identification of the damping. Therefore, the FRFs used were quite possibly contaminated by relatively large leakage errors. Next, we study the effects of variance type random error and leakage error separately to understand how they influence the damping matrix identified by the dynamic stiffness matrix method.

2.2. Effect of variance type measurement error

2.2.1. Numerical study of the effect of the variance type error

A 4 dof lumped parameter system shown in Fig. 5 is used to study the effect of variance type error on the identified damping matrix. The system parameters are defined as $k_1 = k_2 = k_3 = k_4 = 2 \times 10^5\,\text{N/m}$, and

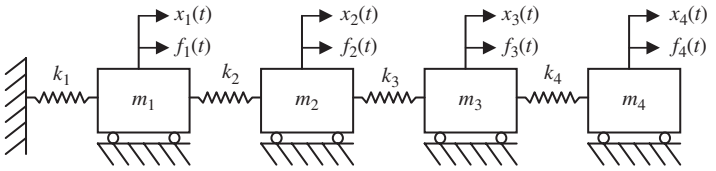

Fig. 5. Lumped parameter system with 4 dofs.

Table 1
Original viscous damping matrix (N s/m)

17.2	−4.9	−0.9	−0.4
−4.9	16.3	−5.4	−1.3
−0.9	−5.4	15.8	−6.3
−0.4	−1.3	−6.3	10.9

$m_1 = m_2 = m_3 = m_4 = 1$ kg. A viscous damping matrix is used which is constructed so that all four modes of the system have a damping ratio of 2% (see Table 1).

Sixteen FRFs are calculated from the model, to which random noises of three different levels, 0.01%, 0.1% and 1% of the dynamic range of the signal are added. These contaminated FRFs are considered as the experimental FRFs. The dynamic stiffness matrix is obtained by inverting the experimental FRF matrix. The imaginary part of the dynamic stiffness matrix is the damping matrix $\mathbf{L}_{\text{exp}}(\omega)$.

Figs. 6(a) and (b) show the magnitude of the fourth diagonal element of the damping matrix and FRF matrix when a 0.01% noise is added. While the FRF shows little trace of the noise, the dynamic stiffness matrix is affected significantly by the noise. Because the exact damping matrix is $\omega\mathbf{C}$, the noise-free damping matrix plotted as a function of frequency should be a straight line. As it is seen in Fig. 6(a), the experimental result is quite scattered around a straight line. This indicates that a curve fitting may be applied to the damping matrix $\mathbf{L}_{\text{exp}}(\omega)$ identified from the dynamic stiffness matrix to eliminate large frequency point-to-point variations. For the viscous damping case, the curve fitting becomes a linear regression [17] as follows:

$$\mathbf{C} = \begin{bmatrix} \omega_1\mathbf{I} \\ \omega_2\mathbf{I} \\ \vdots \\ \omega_k\mathbf{I} \end{bmatrix}^{+}_{kM\times M} \begin{bmatrix} \text{Imag}\left[\mathbf{H}_{\text{exp}}(\omega_1)^{-1}\right] \\ \text{Imag}\left[\mathbf{H}_{\text{exp}}(\omega_2)^{-1}\right] \\ \vdots \\ \text{Imag}\left[\mathbf{H}_{\text{exp}}(\omega_k)^{-1}\right] \end{bmatrix}_{kM\times M}, \tag{4}$$

where "+" represents the pseudo-inverse of the matrix, $\mathbf{I}$ is the identity matrix, and k is the number of frequency points used in the regression. In general, a polynomial curve fitting may be applied to each element of $\mathbf{L}_{\text{exp}}(\omega)$ to obtain the expression of the damping matrix as a function of frequency.

Table 2(a) shows the damping matrix obtained by applying the linear regression (Eq. (4)) to the 0.01% noise case. The identified damping matrix is in a good agreement with the original damping matrix. When the noise level is increased to 0.1%, the plots of the imaginary part of the dynamic stiffness matrix and FRF are given in Figs. 6(c) and (d). The damping matrix is identified in a significantly more scattered form. The $\mathbf{C}$ matrix identified by Eq. (4) shown in Table 2(b) contains large errors. When the noise level is increased to 1%, which is much higher than in typical measured FRFs (see Fig. 6(e)), the noise is almost the same level as the damping ratio, a situation where the object of identification and the noise are similar sized. As expected, the result is completely corrupted as seen in the dynamic stiffness matrix (Fig. 6(f)) and the identified damping matrix (Table 2(c)).

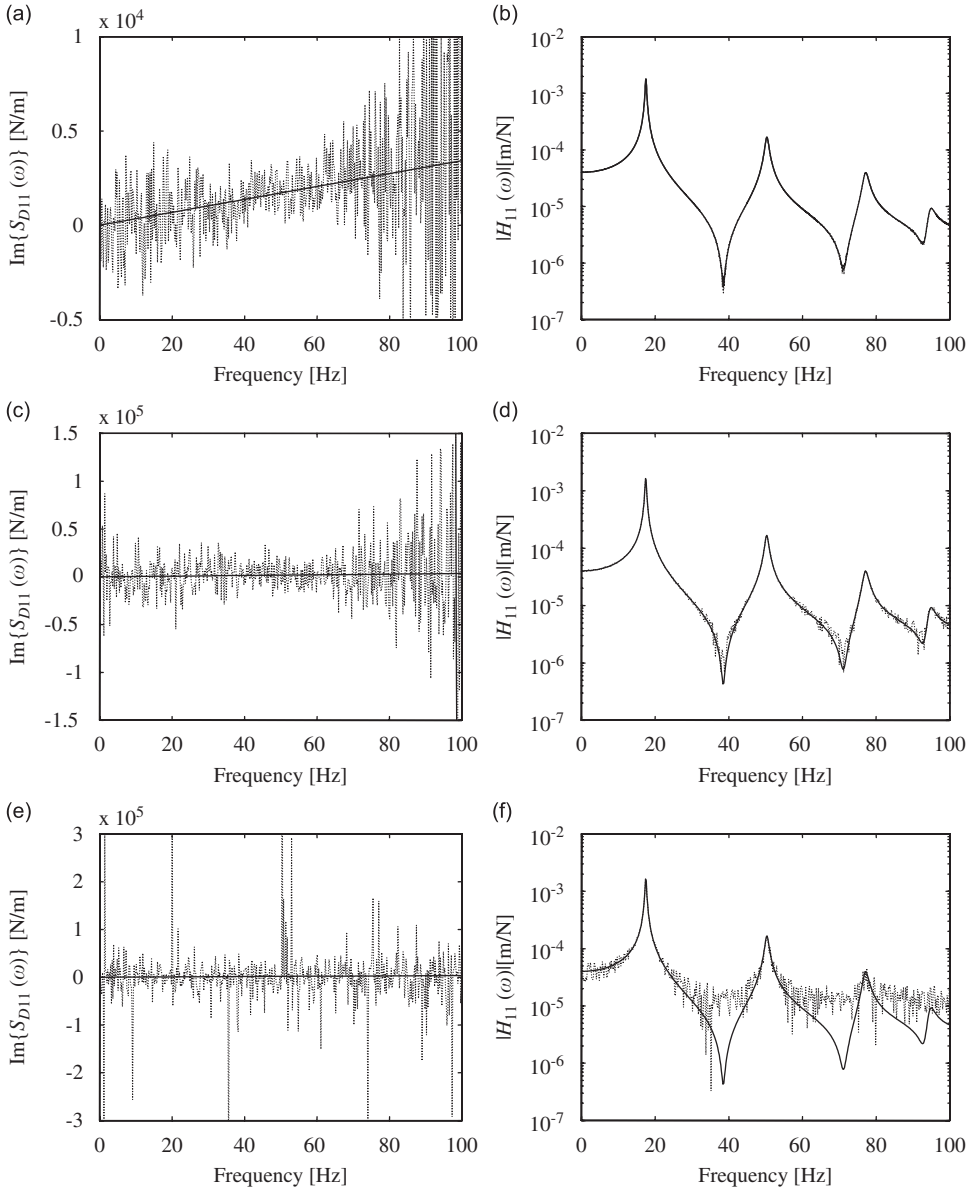

Fig. 6. FRF and dynamic stiffness matrix (DSM) plots for three different signal to noise (S/N) ratios: ——, original; ·····, with noise; (a) imaginary part of 1st diagonal element of the DSM with S/N ratio of 0.01%; (b) Magnitude of the 1st diagonal element of the FRF matrix with S/N ratio of 0.01% ratio; (c) imaginary part of 1st diagonal element of the DSM with S/N ratio of 0.1%; (d) magnitude of the 1st diagonal element of the FRF matrix with S/N ratio of 0.1%; (e) imaginary part of 1st diagonal element of the DSM with S/N ratio of 1%; and (f) magnitude of the 1st diagonal element of the FRF matrix with S/N ratio of 1%.

Table 2
Identified viscous damping matrices (N s/m)

(a) 0.01% error				(b) 0.1% error				(c) 1% error			
17.3	−4.7	−0.9	−0.4	18.5	−3.6	−2.5	−1.5	6.8	4.5	−13.5	6.7
−4.9	16.3	−5.3	−1.3	−4.3	16.8	−5.8	−3.3	−6.6	7.2	4.9	−1.3
−0.6	−5.3	16.1	−6.2	−2.2	−2.4	15.5	−6.3	−9.5	−6.8	17.9	−19.3
−0.5	−1.0	−6.2	10.9	−2.2	−1.1	−4.3	12.5	0.7	7.3	−6.6	5.9

2.2.2. Theoretical study of the effect of the variance type error

We consider the FRF matrix of a linear, time-invariant and viscously damped system described in terms of its modal parameters:

$$\mathbf{H}(\omega)=\sum_{r=1}^{n}\frac{Q_r\boldsymbol{\psi}_r\boldsymbol{\psi}_r^{\mathrm{T}}}{(\mathrm{j}\omega-\lambda_r)}+\frac{Q_r^*\boldsymbol{\psi}_r^*\boldsymbol{\psi}_r^{*\mathrm{T}}}{(\mathrm{j}\omega-\lambda_r^*)}, \tag{5}$$

where $\boldsymbol{\psi}_r$ is the modal vector, complex valued in general, Q_r is the modal scaling factor, and λ_r is the complex modal frequency of the rth mode. The FRF matrix can also be written in an alternative form utilizing the singular value decomposition (SVD) [23] as follows:

$$\mathbf{H}(\omega)=\mathbf{U}(\omega)\boldsymbol{\Sigma}(\omega)\mathbf{V}(\omega), \tag{6}$$

where $\boldsymbol{\Sigma}(\omega)$ is a diagonal matrix called the singular value matrix, and $\mathbf{U}(\omega)$ and $\mathbf{V}(\omega)$ are unitary matrices. Each diagonal element of $\boldsymbol{\Sigma}(\omega)$ represents the contribution of the corresponding column vectors of $\mathbf{U}(\omega)$ and $\mathbf{V}(\omega)$ to the FRF matrix.

Because the dynamic stiffness matrix is the inverse of the FRF matrix, the dynamic stiffness matrix is [18]

$$\mathbf{S}_D(\omega)=\mathbf{V}(\omega)\frac{1}{\boldsymbol{\Sigma}(\omega)}\mathbf{U}(\omega)^H. \tag{7}$$

The singular value decomposition (SVD) and modal parameters are directly related only if the system has a uniform, diagonal mass matrix and a proportional damping matrix. Such a system will be considered in this section to study the effect of variance type errors. We consider that the mass matrix is

$$\tilde{\mathbf{M}}=\alpha\mathbf{I}. \tag{8}$$

Since modal vectors of such a system are real valued and orthogonal to each other, a direct comparison of the FRF in the singular value decomposition and the mode superposition forms becomes possible. First, Eq. (5) is rewritten as

$$\tilde{\mathbf{H}}(\omega)=\sum_{r=1}^{N}\tilde{\boldsymbol{\psi}}_r\tilde{\boldsymbol{\psi}}_r^{\mathrm{T}}\left[\frac{\tilde{Q}_r}{(\mathrm{j}\omega-\lambda_r)}+\frac{\tilde{Q}_r^*}{(\mathrm{j}\omega-\lambda_r^*)}\right], \tag{8'}$$

which is in a matrix form:

$$\tilde{\mathbf{H}}(\omega)=\tilde{\boldsymbol{\psi}}\begin{bmatrix}\frac{\tilde{Q}_1}{(\mathrm{j}\omega-\lambda_1)}+\frac{\tilde{Q}_1^*}{(\mathrm{j}\omega-\lambda_1^*)} & \cdots & 0 & \cdots & 0\\ \vdots & \ddots & \vdots & & \vdots\\ 0 & & \frac{\tilde{Q}_r}{(\mathrm{j}\omega-\lambda_r)}+\frac{\tilde{Q}_r^*}{(\mathrm{j}\omega-\lambda_r^*)} & \cdots & 0\\ \vdots & & \vdots & \ddots & \vdots\\ 0 & \cdots & 0 & \cdots & \frac{\tilde{Q}_N}{(\mathrm{j}\omega-\lambda_N)}+\frac{\tilde{Q}_N^*}{(\mathrm{j}\omega-\lambda_N^*)}\end{bmatrix}\tilde{\boldsymbol{\psi}}^{\mathrm{T}}. \tag{9}$$

Comparing Eqs. (6) and (9), SVD and modal parameters are related as follows:

$$\boldsymbol{\Sigma}(\omega)\propto\begin{bmatrix}\frac{\tilde{Q}_1}{(\mathrm{j}\omega-\lambda_1)}+\frac{\tilde{Q}_1^*}{(\mathrm{j}\omega-\lambda_1^*)} & \cdots & 0 & \cdots & 0\\ \vdots & \ddots & \vdots & & \vdots\\ 0 & \cdots & \frac{\tilde{Q}_r}{(\mathrm{j}\omega-\lambda_r)}+\frac{\tilde{Q}_r^*}{(\mathrm{j}\omega-\lambda_r^*)} & \cdots & 0\\ \vdots & & \vdots & \ddots & \vdots\\ 0 & \cdots & 0 & \cdots & \frac{\tilde{Q}_N}{(\mathrm{j}\omega-\lambda_N)}+\frac{\tilde{Q}_N^*}{(\mathrm{j}\omega-\lambda_N^*)}\end{bmatrix}. \tag{10}$$

Also,

$$\mathbf{U}(\omega), \mathbf{V}(\omega) \propto \tilde{\boldsymbol{\psi}}. \tag{11}$$

Examining Eqs. (6) and (7) in conjunction with Eqs. (10) and (11), it is realized that the mode contributing the least to the FRFs, which therefore has the worst S/N ratio, contributes the most to the dynamic stiffness matrix. In other words, the effect of the measurement noise in the FRF matrix will be highly amplified in the dynamic stiffness matrix because it is dominated by weakest modes. This explains why the dynamic stiffness matrix is tainted much more easily by noise than the FRF matrix; therefore difficult to obtain accurately.

2.2.3. *Variance error analysis with SVD*

Figs. 7 and 8 show the singular values of the FRF and dynamic stiffness matrices of the 4 dof system in Fig. 5 with 0.01% noise. As it is seen in Fig. 7, the lowest two singular values of the FRF matrix are most contaminated throughout the entire frequency range. The contribution of these small singular values becomes very large to the dynamic stiffness matrix as shown in Fig. 8, indicating that the variance noise is amplified in the dynamic stiffness matrix.

The above discussion suggests that reducing the number of singular values will reduce the noise effect in the dynamic stiffness matrix. We consider the dynamic stiffness matrix obtained from a model reduced to a 2 dof system by taking the 2nd and 4th dofs of the original 4 dof model. The singular values of the FRF matrix of the 2 dof reduced model with 0.01% noise are plotted in Fig. 9. Fig. 10(a) shows the second diagonal element

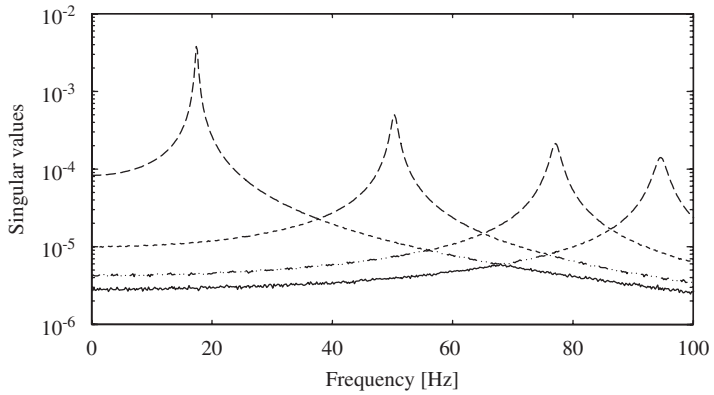

Fig. 7. Singular value plots of the FRF matrix of the 4 dof system: ————, largest singular value; ------, second largest singular value; – · · –, third largest singular value; ——, fourth largest singular value (or lowest).

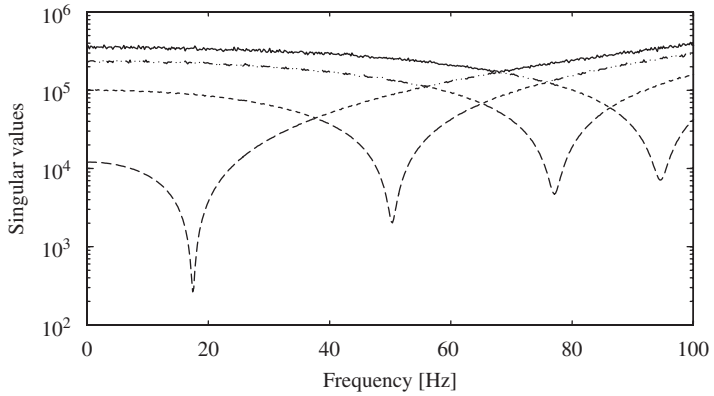

Fig. 8. Singular value plots of the dynamic stiffness matrix of the 4 dof system: ——, largest singular value; – · · –, second largest singular value; ------, third largest singular value; ——, fourth largest singular value (or lowest).

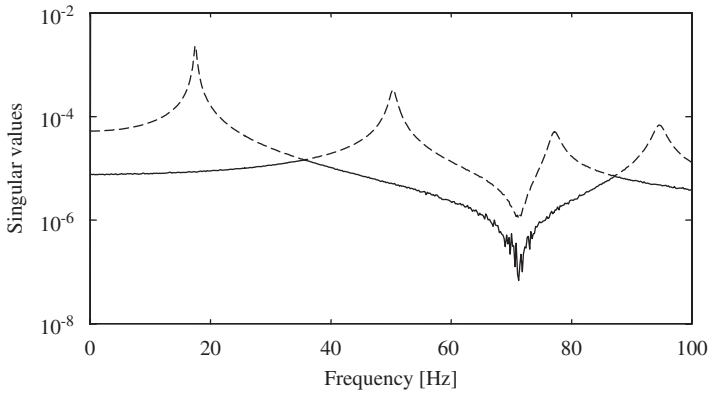

Fig. 9. Singular value plots of the FRF matrix of the 2 dof reduced system: – – – –, largest singular value; ——, second largest singular value (or lowest).

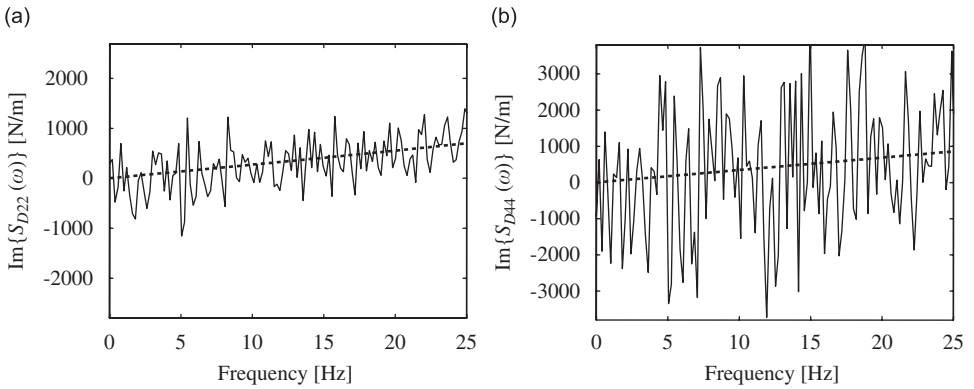

Fig. 10. Diagonal element of the damping matrix identified from the FRF matrix: · · · · · · · ·, original; ——, with noise; (a) 2 dof reduced model and (b) 4 dof original model.

of damping matrix obtained from the 2 dof system, which shows a significant improvement compared to the fourth diagonal element of the damping matrix obtained from the original 4 dof system (see Fig. 10(b)).

In practice, reducing the number of singular values is achieved by decreasing the number experimental dofs, i.e. eliminating some of the dofs, which results in decrease of the size of the dynamic stiffness matrix. While using fewer dofs reduces the error in the dynamic stiffness matrix, it has the obvious disadvantage of reducing the spatial resolution of the experimental model, which may cause that modes in the high frequency range cannot be described. This issue is also discussed as "model incompleteness" by Berman [24–26], and Ozgen and Kim [27,28]. In Refs. [27,28], it is also shown that beyond a certain limiting frequency, the dynamic stiffness matrix obtained from an incomplete reduced model cannot be represented by constant mass and stiffness matrices. Around and beyond this particular frequency limit, it is not possible to represent the system by the reduced experimental model. This limiting frequency has also been related to the lowest anti-resonance frequency observed in the singular value plot of the FRF matrix of the reduced model [28]. In the current case, this frequency is around 70 Hz as seen in the singular value plot of the FRF matrix of the 2 dof reduced model (Fig. 9). To avoid the problem of incompleteness, the identified damping of the 4 and 2 dof models are compared in the frequency range sufficiently lower than the limiting frequency, between 0 and 25 Hz, as seen in Fig. 10.

When applying the dynamic stiffness matrix-based damping identification method, the experimental dofs will have to be selected for a best compromise among the needs for the accuracy of the damping identification,

frequency range and the spatial resolution. This problem can be alleviated to some extent by employing more accurate instrumentation to improve the S/N ratio thus allowing the use of more dofs, and also by adopting a hybrid modeling approach which combines the identified damping matrix of a small number of dofs and the mass and stiffness matrix of much larger dofs formulated experimentally or analytically. The latter requires a procedure to expand the damping matrix, which was reported in Ref. [28].

2.3. Analysis of leakage error

2.3.1. Simulating the leakage error with a numerical model

The leakage error occurs due to the truncation of the time signal [29,30]. The effect of the leakage error can be studied by introducing the error numerically to the FRFs by the following procedure.

(1) Analytic FRFs of the model are calculated from the theoretical model.
(2) The excitation force applied at a particular dof is defined in a random (to simulate random test) or impulsive input (to simulate impact test) in the time domain, and transformed to the frequency domain by applying the fast Fourier transform (FFT).
(3) The response at each dof is calculated in the frequency domain by multiplying the analytic FRF and the force spectrum. In order to be consistent with typical FRF measurement procedures, acceleration responses are used.
(4) The time histories of the acceleration response and force are obtained by applying the inverse FFT (IFFT) to the response and force spectra.
(5) The force and acceleration response data are re-sampled using a slightly smaller block size than the original one, which are transformed back to the frequency domain using FFT. These are numerically altered spectra which include the leakage effect.
(6) The FRF with leakage effect is calculated using H_1 FRF estimation technique [21] using the altered response and force spectra.
(7) The above steps are repeated for all dof, which provides a leakage contaminated FRF matrix.

Using these leakage error added analytical FRFs, the effect of the leakage error can be studied independent of all other effects. In our numerical scheme, we start with the discrete spectra of the response and force in the frequency domain. The inverse FFT is applied to these spectra to obtain time-domain force and response signals, which are assumed to be the signals with no leakage. Then, we change the number of data points, effectively changing the sampling period, which causes the truncation in the time domain.

2.3.2. Examples

We first consider a 6 dof lumped parameter system shown in Fig. 11. The system parameters are defined as $k = 1.0 \times 10^5\,\mathrm{N/m}$, and $m = 1.0\,\mathrm{kg}$. The viscous damping matrix is taken as $\mathbf{C} = 5 \times 10^{-5}\,\mathrm{K}$, which corresponds to modal damping ratios of 0.41%, 0.79%, 1.12%, 1.37%, 1.53%, an average modal damping ratio of 1.04%. The general damping matrix is $\mathbf{L}(\omega) = \omega\mathbf{C}$.

The number of dofs and the boundary conditions of this numerical example are chosen to resemble the experimental model of the aluminum beam tested by Hylok [18]. In order to simulate an impact test case in our numerical example, the force time history is chosen as an impulse function. The frequency range is selected to include all six modes of the system.

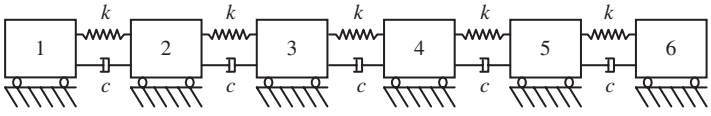

Fig. 11. Lumped parameter model with 6 dofs.

The spatial plot of the imaginary part of the dynamic stiffness matrix obtained by using the leakage contaminated FRFs is shown in Fig. 12. It is clearly seen that the diagonal elements of the damping matrix $\mathbf{L}(\omega)$ become negative in a wide frequency range as it was observed in experimental results (see Fig. 4). Figs. 13(a) and (b) compare the first diagonal elements of the experimentally identified damping matrix shown in Fig. 4 with the damping matrix identified from the numerical model in Fig. 12. Fig. 14 compares the singular values of the FRF matrix of the theoretical model in Fig. 11 obtained with and without the simulated leakage effect. It is seen that the leakage error affects the singular values in the lower frequency range significantly. This observation supports the hypothesis that the leakage error is the main source of the bias error in the dynamic stiffness matrix-based damping identification.

In order to further support our findings, the leakage error was introduced to FRFs obtained from a finite element analysis (FEA) model. This model was correlated with the aluminum beam used by Hylok [18] in an approximate sense by matching FRF amplitudes and resonant frequencies obtained from the model with those from the test model. In addition to leakage error, a small level of variance error was introduced into the FRFs obtained from the FEA model. The spatial plot of the damping matrix obtained from the FEA model is shown in Fig. 15. It can be seen that the distortions in this damping matrix caused by the simulated leakage and variance errors resemble the distortions observed in Fig. 4 obtained from the experimental model. This further supports the hypothesis that in the identified damping the leakage error distorts the envelope and the random error makes the data points scattered.

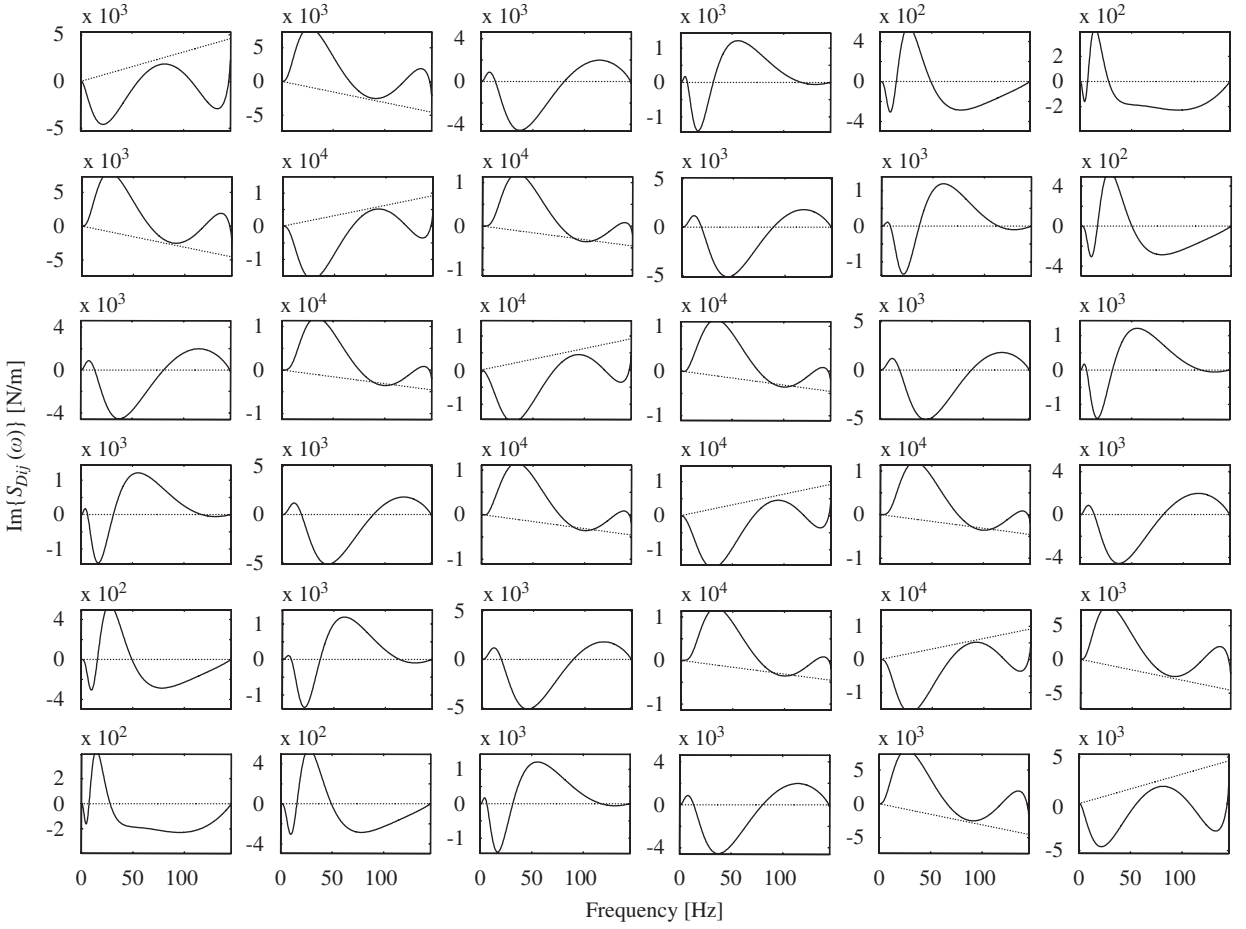

Fig. 12. Spatial plot of the imaginary part of the dynamic stiffness matrix of the 6 dof system: ·····, original; ——, with simulated leakage.

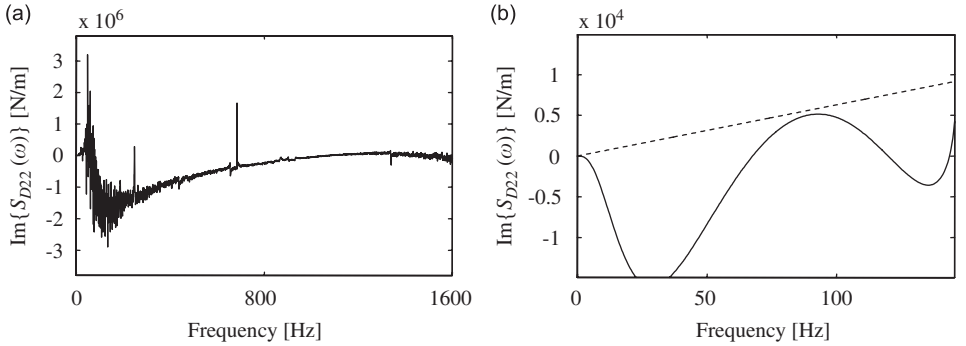

Fig. 13. Second diagonal element of the damping matrix: (a) for Hylok's aluminum beam [18] and (b) for the 6 dof numerical model: ------, original; ——, with simulated leakage.

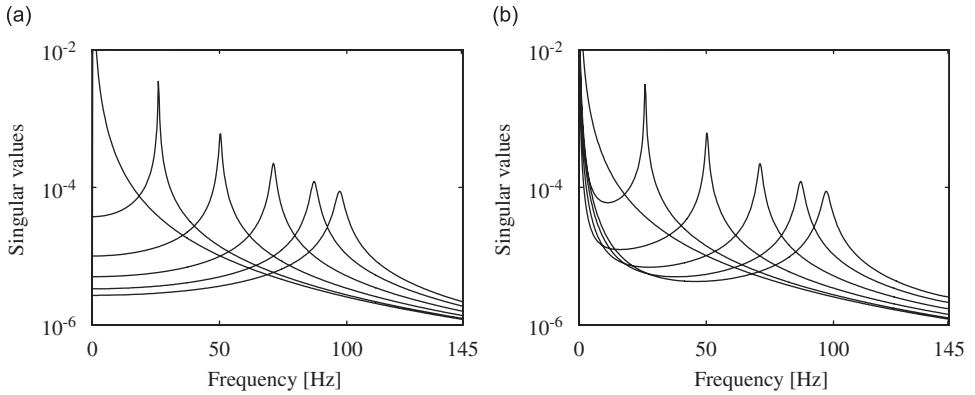

Fig. 14. Singular value plots of the FRF matrix of the 6 dof model: (a) original and (b) with simulated leakage.

3. Practical feasibility of the dynamic stiffness matrix-based damping identification

It was seen that the dynamic stiffness matrix-based damping identification was highly vulnerable to experimental errors. This leads to an obvious question: "Is the dynamic stiffness matrix method a practically feasible method?" We constructed very simple test set-ups and applied test procedures devised to minimize both the variance type and bias errors to answer this question.

3.1. Minimizing effects of measurement errors

If a random input testing is used, a large number of spectral averaging can be used to minimize the variance type errors. Proper selection of sensors and the dynamic range for the data acquisition process will also reduce the effect of variance errors by improving the S/N ratio. The random input testing method can employ various time windows, cyclic averaging, and special input force functions like burst random, pseudo-random inputs, which can minimize leakage errors efficiently.

An exponential window cannot be used with the impact test to reduce the leakage error because it introduces an artificial damping effect [22]; therefore is not a good choice for the dynamic stiffness matrix-based damping identification in general. The method can be used if the system is highly damped, as it will be demonstrated in this paper. Using cyclic averaging may also be a remedy for the leakage effect when working with lightly damped systems.

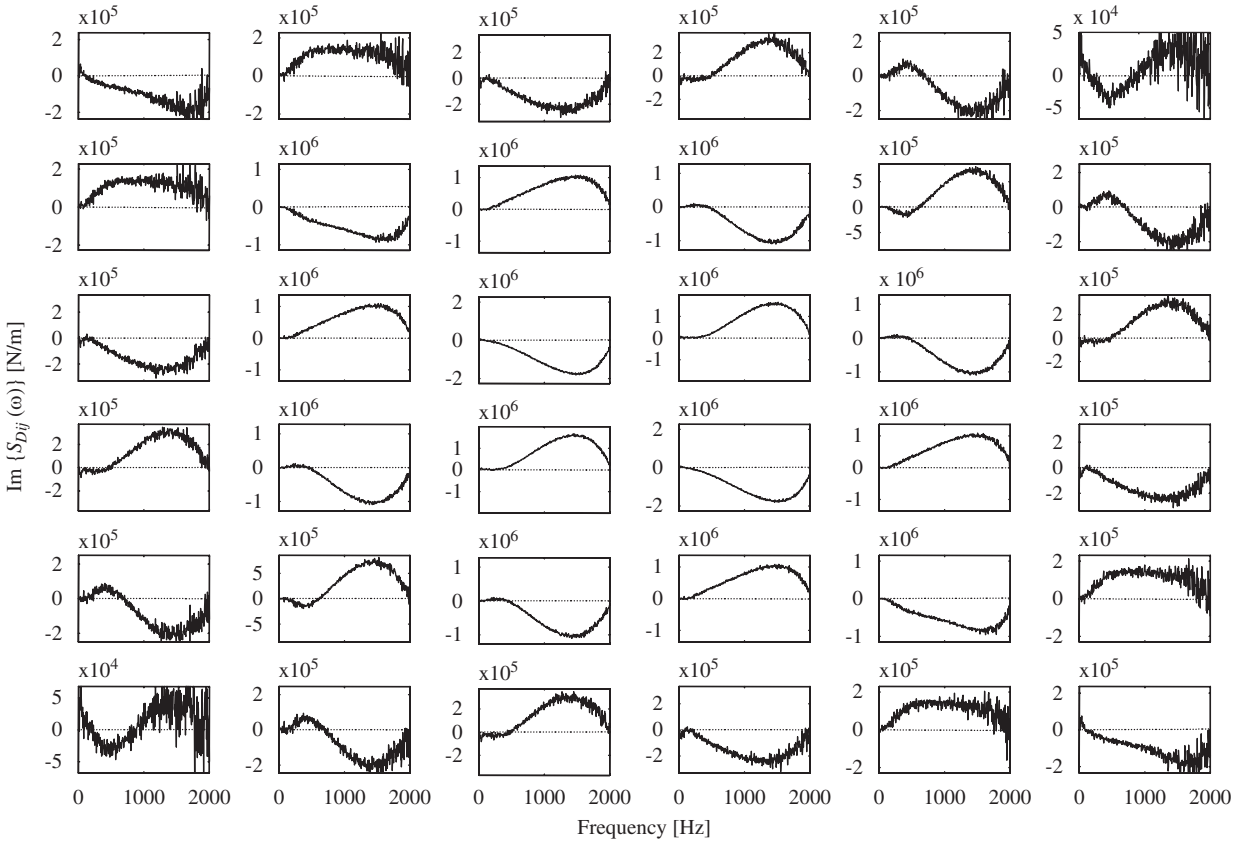

Fig. 15. Spatial plot of the imaginary part of the dynamic stiffness matrix of the beam FEA model: ·····, original; ——, with simulated leakage and variance errors.

3.2. Application of the improved test procedure

3.2.1. Damped suspended block

In a previous work by the authors [19], a damping matrix was identified on a very simple 2 dof system: a rigid block suspended by two thin composite beams. The setup in Ozgen and Kim's work [19] can be approximated as a rigid mass suspended by two complex springs. The structure is excited with random inputs at the two ends of the rigid block using two small shakers. Hanning window and cyclic averaging were used to minimize the leakage error. All diagonal elements of the identified damping matrix $\mathbf{L}_{\text{exp}}(\omega)$ of this two dof system obtained were positive valued. The off-diagonal elements of the identified damping matrix were negative valued, which is the expected form of a typical damping matrix of a 2 dof system. Results presented in Ref. [19] show that identifying the damping matrix from the dynamic stiffness matrix is feasible for a simple system. The feasibility of the method for a more complicated system is discussed in the following section.

3.2.2. Damped beam

An aluminum beam was constructed to apply the dynamic stiffness matrix-based damping identification to a more realistic system. The beam has dimensions similar to what Hylok used [18], but damping in the beam was significantly increased by applying constrained layer damping treatments on both surfaces. Twelve measurement points were chosen at equally spaced locations along the longitudinal axis of the beam. Pictures of the setup are shown in Figs. 16(a)–(c). The accelerometers were stud-mounted on aluminum mounts super glued to the beam surface, placed on both surfaces so that the force can be applied in a symmetric fashion. Both impact test and random input test were used in this case.

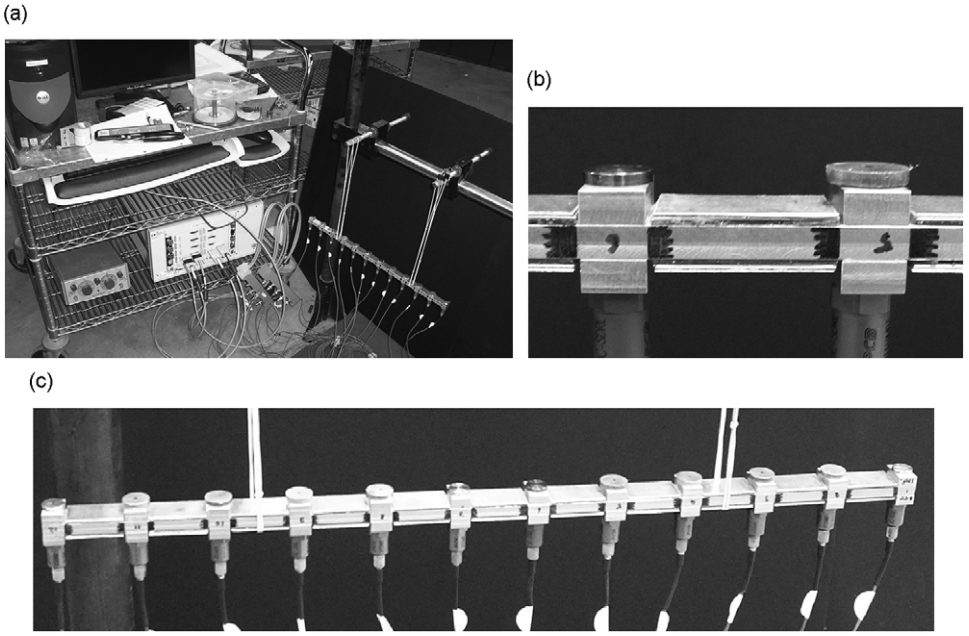

Fig. 16. Damped aluminum beam—test setup: (a) overall view, (b) close-up view of response measurement points, and (c) beam with accelerometers.

3.2.2.1. Impact test. The impact test may be applicable because the system is quite highly damped; therefore the response is nearly fully observable without using an exponential window. The frequency range is selected to include the first 3 modes. A 4×4 subset of the measured FRF matrix corresponding to the first 4 dofs is shown in Fig. 17, which look quite clean. Fig. 18 shows the spatial plot of the first 4×4 subset of the imaginary part of the dynamic stiffness matrix which shows traces of large variance errors. The plot of the twelve singular values of the FRF matrix is shown in Fig. 19. Having these many singular values, quite a few singular values are expected to be very small, possibly below the noise floor, which will heavily contaminate the dynamic stiffness matrix with noise.

To reduce the number of singular values, a 6 dof model is constructed by selecting every other dof from the initial 12 dofs as shown in Fig. 20. In order to show the improvement over the 12 dof case, the imaginary part of one of the diagonal elements of the dynamic stiffness matrix of the 6 dof model is plotted in Fig. 21. When compared to the 12 dof case in Fig. 18, the plot shows a dramatic improvement. The imaginary part is positive valued at most frequency points and increases linearly as a function of the frequency similar to the viscous damping case. This improvement can be attributed to the fact that the impact responses were almost fully observable within the sampling period because of the high damping, which limits the leakage error to make the impact test acceptable.

Because $T = 1/\Delta f$, where T is the sampling period and Δf is the frequency increment, the sampling period can be reduced by using a larger frequency increment. In this case, the impact responses do not fully decay out, causing the leakage error [22]. The number of time points used in a second set of FRF measurements is reduced this way to 200 from 1600 that was used in the initial impact test. In Fig. 22, the spatial plot of the imaginary parts of the dynamic stiffness matrices of the two cases (200 and 1600 points) are compared. The same effect of the leakage on the imaginary parts of the dynamic stiffness matrix observed in the numerical simulations of Section 2.3.2 is also observed here (for comparison see Figs. 12, 13 and 15).

Note that in Fig. 22 for the leakage-free case (based on measurements with 1600 frequency points), several spikes are observed at certain frequencies such that diagonal elements of the identified damping matrix become negative. The frequencies at which these spikes occur can be explained from the singular values of the FRF matrix shown in Fig. 23. In addition to the three resonant peaks contained in the range, lower singular values have very small peaks at the frequencies where the damping elements have spikes. These small peaks

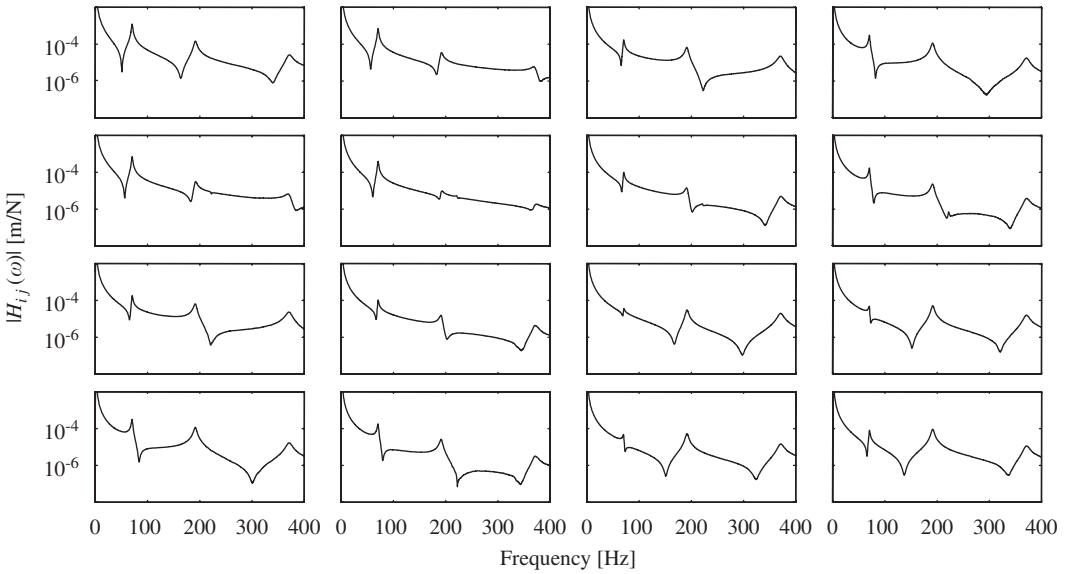

Fig. 17. Spatial plot of the 4×4 subset of the FRF matrix associated with the first 4 dofs of the damped aluminum beam (12 dof experimental model—impact test results).

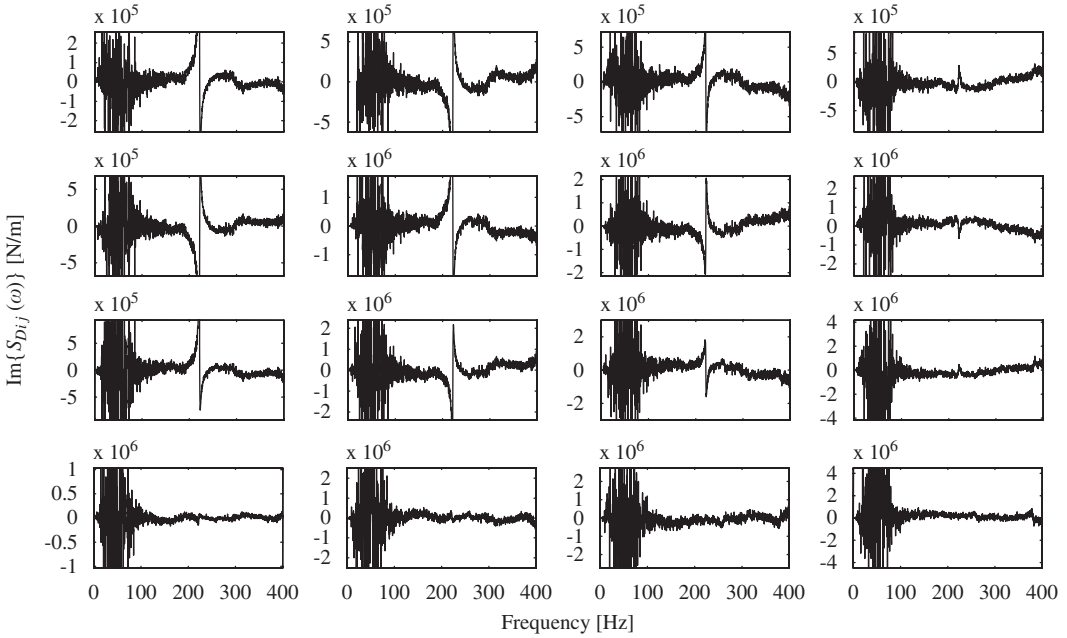

Fig. 18. Spatial plot of the 4×4 subset of the dynamic stiffness matrix (imaginary part) associated with the first 4 dofs of the damped aluminum beam (12 dof experimental model-impact test results).

may be associated with the modes that could not be captured by the experiment, for example a torsional mode although it has to be proved. The effect of these un-captured modes is very small in the FRFs; however significant in the dynamic stiffness matrix.

3.2.2.2. Random input test. Random input testing is expected to provide a better accuracy for dynamic stiffness matrix than the impact testing because it is easier to control variance and bias type errors. A square

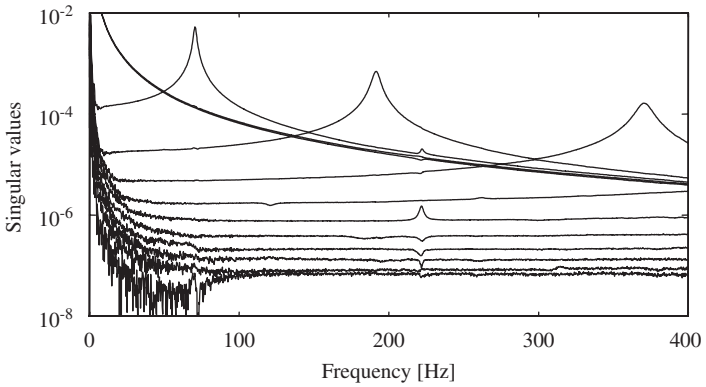

Fig. 19. Singular value plots of the FRF matrix of the damped aluminum beam (12 dof experimental model-impact test results).

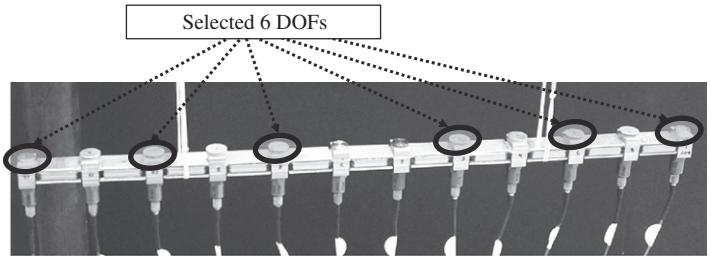

Fig. 20. The dofs selected among the 12 dof test setup of the damped aluminum beam to construct a reduced size 6 dof experimental model.

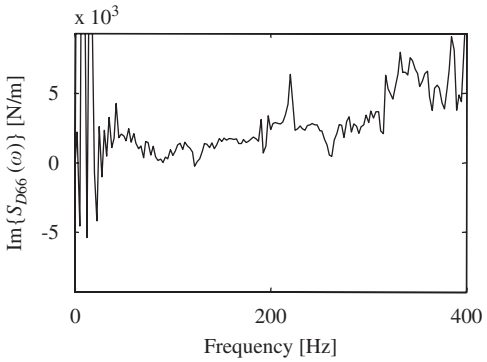

Fig. 21. Sixth diagonal element of the damping matrix (imaginary part of the dynamic stiffness matrix) of the damped aluminum beam (6 dof experimental model-impact test results).

FRF matrix can be obtained by the single input–multi-output (SIMO) testing [31], which uses a single shaker to excite the structure with a similar procedure to the MRIT. However in the case of our test object, the mass loading caused by the force transducer attached between the shaker stringer and the structure adversely affected the dynamic stiffness matrix results. FRFs were obtained slightly differently depending on the excitation point because of the mass loading effect of the shaker. This problem, while it is insignificant in modal analysis, becomes significant in the dynamic stiffness matrix-based damping identification. The multi-input–multi-output (MIMO) testing [31] can eliminate this problem.

The MIMO testing was applied using 5 dofs, which were limited by the available shakers. All 12 accelerometers used in the impact testing of the damped beam were kept on the structure to make the system as close as possible to what was used in the impact testing. The setup is shown in Figs. 24(a)–(c). The singular

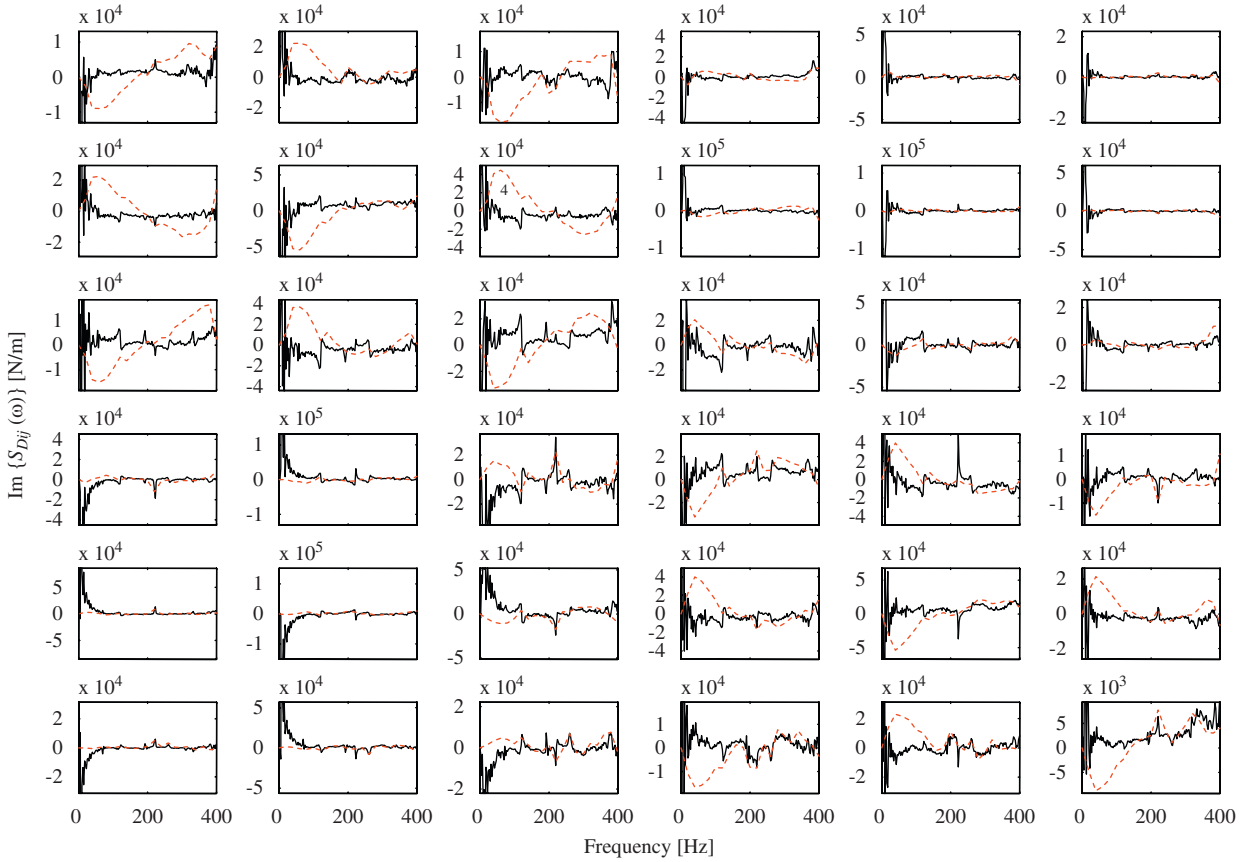

Fig. 22. Spatial plot of the imaginary part of the dynamic stiffness matrix of the damped aluminum beam (6 dof experimental model-impact test results): ——, 1600 frequency points; --------, 200 frequency points (increased leakage error).

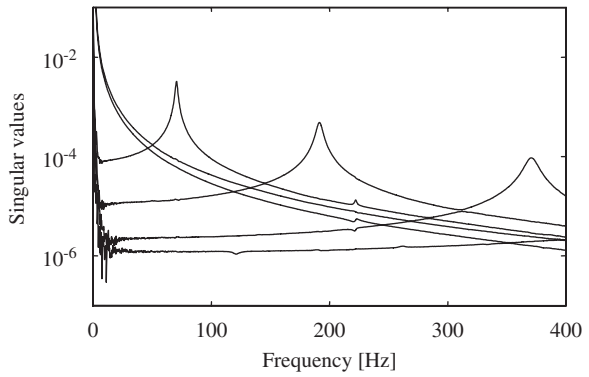

Fig. 23. Singular value plots for the FRF matrix of the damped aluminum beam (6 dof experimental model—impact test results).

value plots of the FRF matrix in Fig. 25 obtained from the random test show a weak fourth mode around 225 Hz, which may be related to an un-measured torsional mode.

In Fig. 26, the spatial plot of the 5×5 FRF matrix obtained from the random input test is compared with the corresponding subset of the FRF matrix obtained from the impact test. The comparison shows that the frequencies of the three major modes obtained by the MIMO test are slightly lower than those obtained by the impact test, indicating the mass loading effect of the shakers and force transducers. The imaginary part of

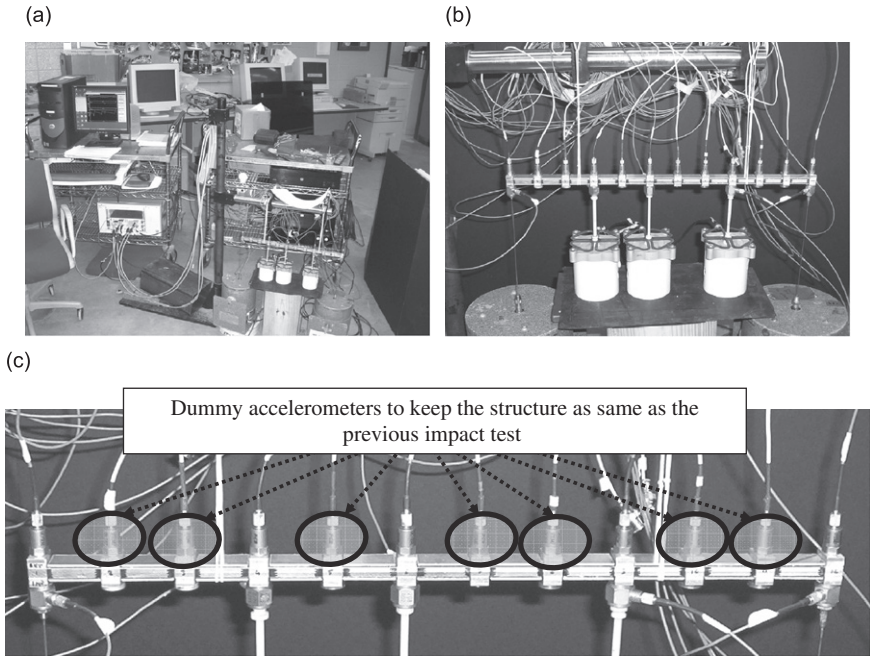

Fig. 24. Test setup for the MIMO testing of the damped aluminum beam: (a) overall view, (b) close-up view of the beam and the shakers, and (c) close-up view of sensor configuration.

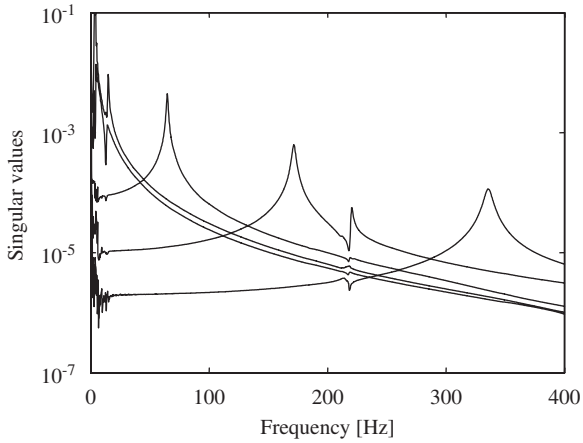

Fig. 25. Singular value plots of FRF matrix of the damped aluminum beam (5 dof experimental model—MIMO random input test).

the dynamic stiffness matrix obtained from the impact and random tests are compared in the spatial plot form in Fig. 27. Imaginary parts of the dynamic stiffness, thus the experimental damping matrices are in a very good agreement. This indicates that the damping in the system was not significantly affected by the mass loading effect of the shaker stringers and force transducers. The main difference is observed around the resonance frequency at 225 Hz, which causes sharper peaks in the random test results as seen in Fig. 27.

The damping matrix identified from the random testing shows a significant improvement from the matrix obtained from the impact testing. The random input test result shows a smoother and more linear frequency distribution without the distortion, a sign of leakage error.

3.2.2.3. Validation of the identified damping matrix $\boldsymbol{L}_{exp}(\omega)$. In order to verify the accuracy of the experimental procedure, the damping matrix of the damped beam obtained by using the dynamic stiffness

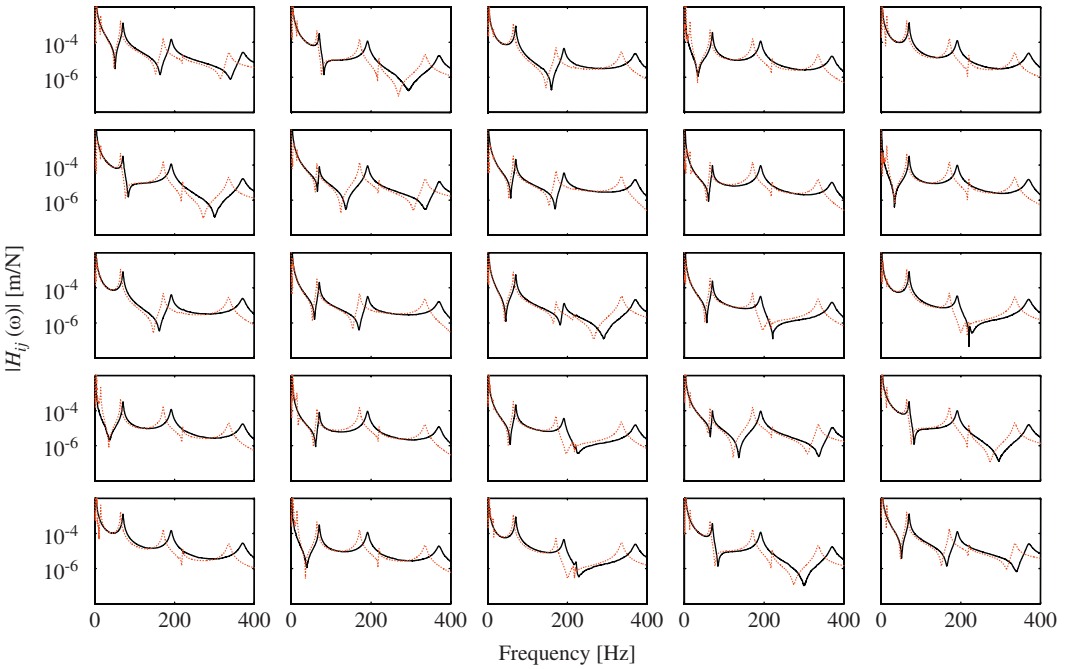

Fig. 26. Spatial plot of the FRF matrix of the damped aluminum beam (5 dof experimental model): ——, impact test results; ·····, MIMO test results.

matrix method and the damping matrix obtained by another method (inverse approach) are compared. The inverse approach assumes that the system is proportionally damped; therefore [32]:

$$\boldsymbol{\psi}^{\mathrm{T}}\mathbf{C}\boldsymbol{\psi} = \begin{bmatrix} 2\xi_1\Omega_1 M_1 & 0 & 0 \\ 0 & \ddots & 0 \\ 0 & 0 & 2\xi_N\Omega_N M_N \end{bmatrix}, \tag{12}$$

where ξ_i is the damping ratio, M_i is the modal mass, and $\boldsymbol{\Omega}_i$ is the undamped modal frequency of the ith mode. Pre- and post-multiplying Eq. (12) by $(\boldsymbol{\psi}^{\mathrm{T}})^{-1}$ and $(\boldsymbol{\psi})^{-1}$, the damping matrix $\mathbf{C}$ is obtained as follows:

$$\mathbf{C} = (\boldsymbol{\psi}^{\mathrm{T}})^{-1}\begin{bmatrix} 2\xi_1\Omega_1 M_1 & 0 & 0 \\ 0 & \ddots & 0 \\ 0 & 0 & 2\xi_N\Omega_N M_N \end{bmatrix}(\boldsymbol{\psi})^{-1}. \tag{13}$$

In this equation, the damping ratios (ξ_I's) should be obtained from experiments while modal masses (M_i's) and the undamped modal frequencies (Ω_I's) may be obtained either experimentally or analytically. Eq. (13) can be used only when $\boldsymbol{\psi}$ is a square matrix; therefore, the number of the modes and dofs of the experimental model should be equal.

The proportional damping matrix estimated for the damped beam using Eq. (13) can be used to compute the imaginary part of dynamic stiffness matrix of the system, which is simply equal to $\omega\mathbf{C}$. This damping matrix distribution can then be directly compared to $\mathbf{L}_{\mathrm{exp}}(\omega)$, the damping matrix obtained from the dynamic stiffness matrix-based approach. Damping matrix comparison as described will be made for the 5 dof experimental model of the damped beam which was used in Section 3.2.2.2. As we need a square modal matrix to utilize Eq. (13), we need the first five modes of the system. The measured system is a free–free beam and the first two modes are rigid body modes with near-zero frequencies, which usually cannot be extracted from the FRF data. Because of the lack of modal information for all five modes, Eq. (13) cannot be utilized based on the modal information obtained solely from experimental modal analysis. In this case, modal masses and modal frequencies will have to be obtained from the mass and stiffness matrices of the 5 dof experimental

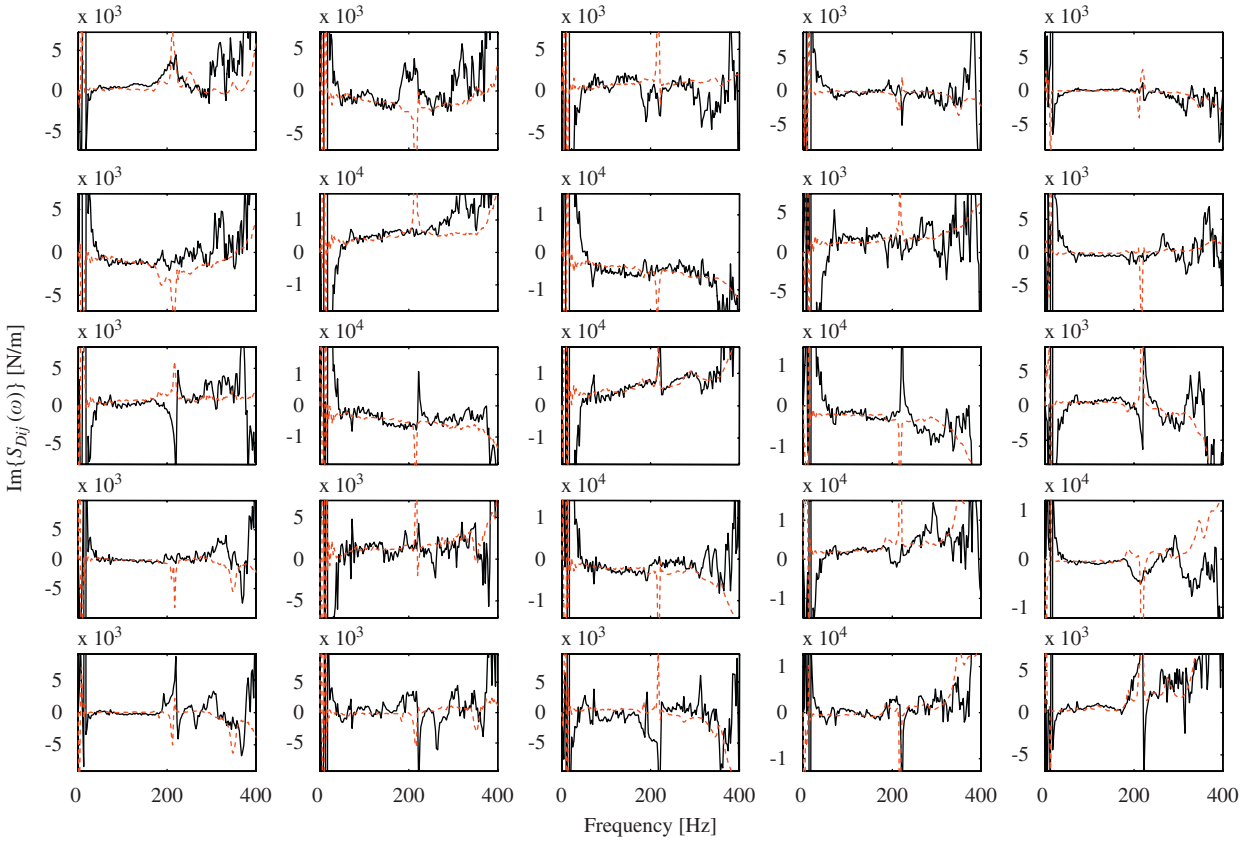

Fig. 27. Spatial plot of the imaginary part of the dynamic stiffness matrix of the damped aluminum beam (5 dof experimental model): ——, impact test results; --------, MIMO test results.

model while modal damping ratios will have to be obtained from modal analysis of the experimental FRF data. For the mass and stiffness matrices, we use $\mathbf{M}_{\text{exp}}$ and $\mathbf{K}_{\text{exp}}$,, the mass and stiffness matrices obtained also from experiment, which are:

$$\begin{bmatrix} \mathbf{K}_{\text{exp}} \\ \mathbf{M}_{\text{exp}} \end{bmatrix}_{2M\times M} = \begin{bmatrix} \mathbf{I} & -\omega_1^2\mathbf{I} \\ \mathbf{I} & -\omega_2^2\mathbf{I} \\ . & . \\ . & . \\ \mathbf{I} & -\omega_k^2\mathbf{I} \end{bmatrix}^{+}_{kM\times 2M} \begin{bmatrix} \text{Real}[\mathbf{H}_{\text{exp}}(\omega_1)^{-1}] \\ \text{Real}[\mathbf{H}_{\text{exp}}(\omega_2)^{-1}] \\ . \\ . \\ \text{Real}[\mathbf{H}_{\text{exp}}(\omega_k)^{-1}] \end{bmatrix}_{kM\times M}, \tag{14}$$

where "+" represents the pseudo-inverse of the matrix.

$\mathbf{M}_{\text{exp}}$ and $\mathbf{K}_{\text{exp}}$ of the 5 dof experimental model of the damped beam obtained from Eq. (14) are given in Tables 3 and 4, respectively. Modal damping ratios for the same experimental configuration are found as 0.013, 0.012 and 0.013 for the first three structural modes at frequencies 443.6, 1203.8 and 2329.3 rad/s, respectively. As the two rigid body modes are not identifiable, a modal damping ratio of 0.01 was taken for these two modes. Using the experimental system matrices $\mathbf{M}_{\text{exp}}$ and $\mathbf{K}_{\text{exp}}$, modal masses M_i's and undamped modal frequencies Ω_I's are computed. Finally Eq. (13) can be used to calculate the proportional damping matrix $\mathbf{C}_{\text{exp}}$, which is the damping matrix identified in the conventional way assuming proportional damping. This proportional damping matrix is shown in Table 5.

Comparison of $\omega\mathbf{C}_{\text{exp}}$ and the imaginary part of $\mathbf{L}_{\text{exp}}(\omega)$ obtained from the dynamic stiffness matrix-based approach can be seen in Fig. 28. The results compare well in terms of the magnitude while the actual

Table 3
Identified mass matrix (kg)

0.0474	0.0201	−0.0021	0.0005	0.0005
0.0195	0.1261	−0.0299	0.0010	0.0025
−0.0064	−0.0248	0.1145	0.0105	−0.0078
0.0023	−0.0025	0.0083	0.1142	0.0182
−0.0009	0.0035	−0.0095	0.0171	0.0483

Table 4
Identified stiffness matrix (N/m)

21,315	−61,106	46,325	−7267	1203
−59,365	220,804	−218,592	69,037	−11,769
45,125	−219,908	278,144	−137,030	33,624
−7214	69,359	−136,535	115,487	−40,054
1426	−12,398	34,907	−41,706	17,564

Table 5
Identified proportional damping matrix (N s/m)

0.456	−0.722	0.244	0.051	0.061
−0.722	2.855	−2.485	0.456	0.033
0.244	−2.485	3.716	−1.584	0.188
0.051	0.456	−1.584	1.889	−0.683
0.061	0.033	0.188	−0.683	0.433

distributions are obviously different because the actual damping is not proportional. This comparison serves as a qualitative validation of the accuracy of the dynamic stiffness-based damping identification.

4. Summary and conclusion

Among various approaches proposed to obtain damping matrices based on experimental measurement, the dynamic stiffness matrix (DSM)-based damping identification method proposed by Lee and Kim [17] is attractive because it has a very simple algorithm and does not use any unfounded assumptions or simplifications. However, it was observed that the damping matrices identified by the method showed unexpected forms with traces of large experimental errors. In this work, the sources of this problem are investigated and an improved experimental procedure is developed.

The dynamic stiffness matrix-based approach finds the damping matrix from the dynamic stiffness matrix of the system, which is obtained by inverting the measured FRF matrix. It is shown that variance errors in the measured FRFs are greatly magnified in the inversion process, heavily contaminating the identified damping matrix. It is shown that the effect of the variance error on the damping matrix can be related to the lowest singular values of the FRF matrix, in turn the dofs of the experimental model; therefore the smaller the measurement dofs are, the smaller the variance error becomes. This indicates that the size of dofs has to be selected in the measurement as a compromise between the needs for the spatial resolution and the accuracy of the damping matrix. A model expansion method developed previously by the authors [28] partially relaxes this dilemma because it can expand the identified damping matrix to a larger size. Observing the patterns of identified damping matrices in previous works indicates the existence of an error of different type in addition to the more obvious variance error. A hypothesis is made that this additional error is the leakage error in the FRF measurement, which is confirmed by numerical simulations of lumped parameter systems and a finite element analysis model.

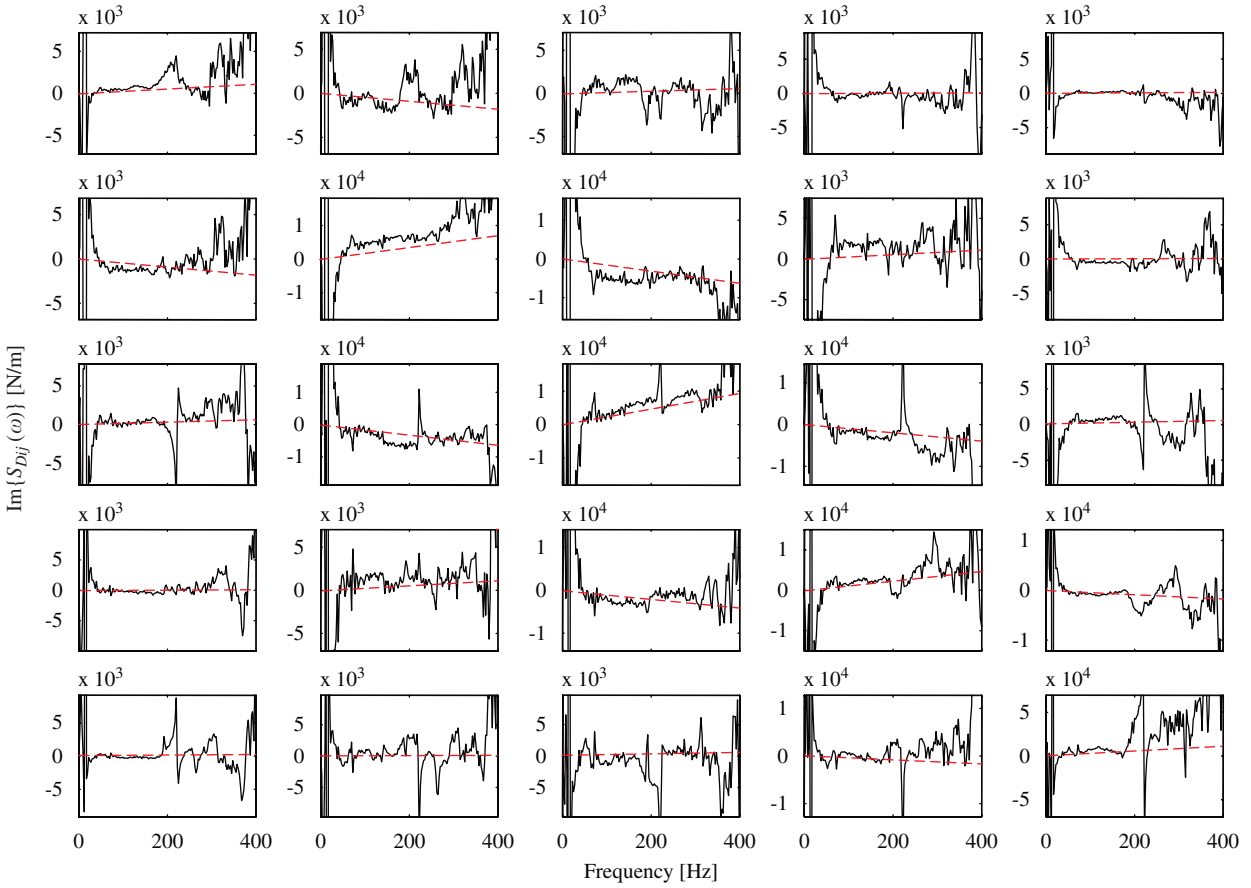

Fig. 28. Spatial plot of the imaginary part of the dynamic stiffness matrix of the damped aluminum beam (5 dof experimental model): ——, dynamic stiffness-based method; - - - - - - - -, inverse method for proportionally damped systems.

The MIMO random input test is the experiment of choice for the dynamic stiffness matrix approach because it enables minimizing both variance and leakage type errors. An experimental procedure based on the MIMO test was previously applied to a very simple experimental set-up composed of only 2 dofs to verify the practicality of the dynamic stiffness matrix approach [19]. In this previous work [19], the damping matrix was obtained in a well-expected form with a trace of only modest variance errors. In this current study, the procedure is also applied to a more realistic system, a cantilever beam described by five measurement dofs, which identifies the damping matrix in a well-explainable form. These experiments suggest that the dynamic stiffness matrix-based approach can be a practical option in modeling dynamic systems.

Simple damping models have been used for a long time because not only there was no alternative but also they offered acceptable accuracy for most engineering tasks. Therefore, it will be an interesting task to find specific types of problem in that an accurate damping matrix description is crucial. Interestingly, such a study has never been conducted while numerous efforts have been reported about developing damping matrix formulation. Developing measurement techniques to further reduce the variance error is another necessary and more obvious future task, which will expand the practicality of the dynamic stiffness matrix-based method.

References

[1] M. Link, Identification of physical system matrices using incomplete vibration test data, *Proceedings of the 4th International Modal Analysis Conference*, Los Angeles, CA, 1986, pp. 386–393.

[2] M. Link, M. Weiland, J.M. Barragán, Direct physical matrix identification as compared to phase resonance testing: an assessment based on practical application, *Proceedings of the 5th International Modal Analysis Conference*, Vol. 1, London, UK, 1987, pp. 804–811.
[3] Y.W. Luk, Identification of physical mass, stiffness and damping matrices using pseudo-inverse, *Proceedings of the Fifth International Modal Analysis Conference*, Vol. 1, London, UK, 1987, pp. 679–685.
[4] K. Shye, M. Richardson, Mass, stiffness, and damping matrix estimates from structural measurements, *Proceedings of the Fifth International Modal Analysis Conference*, Vol. 1, London, UK, 1987, pp. 756–761.
[5] N.G. Creamer, J.L. Junkins, Identification method for lightly damped structures, *Journal of Guidance* 11 (6) (1988) 571–576.
[6] W.F. Tsang, E. Rider, The technique of extraction of structural parameters from experimental forced vibration data, *Proceedings of the Seventh International Modal Analysis Conference*, Vol. 2, Las Vegas, NV, 1989, pp. 1627–1633.
[7] J.L. Jensen, R. Brincker, A. Rytter, Identification of light damping in structures, *Proceedings of the Eighth International Modal Analysis Conference*, Vol. 2, Kissimmee, FL, 1990, pp. 1041–1047.
[8] D.F. Pilkey, D.J. Inman, An iterative approach to viscous damping matrix identification, *Proceedings of the 15th International Modal Analysis Conference*, Vol. 1, Orlando, FL, 1997, pp. 104–110.
[9] D.F. Pilkey, P. Gyuhae, D.J. Inman, Damping matrix identification and experimental verification, *Smart Structures and Materials, SPIE Conference on Passive Damping and Isolation*, Newport Beach, CA, 1999, pp. 350–357.
[10] S. Adhikari, J. Woodhouse, Towards identification of a general model of damping, *Proceedings of the 18th International Modal Analysis Conference*, Vol. 1, San Antonio, TX, 2000, pp. 377–383.
[11] D.J. Henwood, Approximating the hysteretic damping matrix by a viscous matrix for modeling in the Time Domain, *Journal of Sound and Vibration* 254 (3) (2002) 575–593.
[12] S.R. Ibrahim, W. D'ambrogio, P. Salvini, A. Sestieri, Direct updating of nonconservative finite element models using measured input–output, *Proceedings of the 10th International Modal Analysis Conference*, Vol. 1, San Diego, CA, 1992, pp. 202–210.
[13] S. Lammens, M. Brughmans, J. Leuridan, P. Sas, Application of a FRF based model updating technique for the validation of finite element models of components of the automotive industry, *Proceedings of the 1995 Noise and Vibration Conference*, Vol. 1, SAE International, Traverse City, MI, 1995, pp. 103–115.
[14] S.Y. Chen, M.S. Ju, Y.G. Tsuei, Stiffness and damping matrices from frequency response functions, *ASME Journal of Vibration and Acoustics* 118 (1996) 78–82.
[15] M. Dalenbring, Damping function estimation based on measured vibration frequency responses and finite-element displacement modes, *Mechanical Systems and Signal Processing* 13 (1999) 547–569.
[16] J.H. Lee, J. Kim, Identification of damping matrices from measured frequency response functions, *Journal of Sound and Vibration* 240 (3) (2001) 545–565.
[17] J.H. Lee, J. Kim, Development and validation of a new experimental method to identify damping matrices of a dynamic system, *Journal of Sound and Vibration* 246 (3) (2001) 505–524.
[18] J.E. Hylok, Experimental Identification of Distributed Damping Matrices using the Dynamic Stiffness Matrix, M.S. Thesis, University of Cincinnati, 2002.
[19] G.O. Ozgen, J. Kim, Further developments in the dynamic stiffness matrix (DSM) based direct damping identification method, *SAE 2005 Transactions, Journal of Passenger Cars-Mechanical Systems* (2006) 2704–2712.
[20] W.A. Fladung Jr., D.L. Brown, Multiple reference impact testing, *Proceedings of the 11th International Modal Analysis Conference*, Vol. 2, Orlando, FL, 1993, pp. 1221–1229.
[21] R.J. Allemang, *Vibrations: Experimental Modal Analysis*, UC-SDRL-CN-20-263-663/664, Structural Dynamics Research Laboratory, University of Cincinnati, 1999.
[22] B. Fladung, Windows used for impact testing, *Proceedings of the 15th International Modal Analysis Conference*, Vol. 2, Orlando, FL, 1997, pp. 1662–1666.
[23] W. To, D. Ewins, The role of the generalized inverse in structural dynamics, *Journal of Sound and Vibration* 186 (2) (1995) 185–195.
[24] A. Berman, System identification of structural dynamic models—theoretical and practical bounds, *AIAA/ASME/ASCE/AHS 25th Structures, Structural Dynamics & Materials Conference*, Vol. 2, Palm Springs, CA, 1984, pp. 123–129.
[25] A. Berman, Validity of improved mathematical models, s commentary, *Proceedings of the 16th International Modal Analysis Conference*, Vol. 1, Santa Barbara, CA, 1998, pp. 681–691.
[26] A. Berman, Inherently incomplete finite element model and its effects on model updating, *AIAA Journal* 38 (11) (2000) 2142–2146.
[27] G.O. Ozgen, J. Kim, Applications of the dynamic stiffness matrix (DSM) based direct damping identification method, *SAE 2005 Noise and Vibration Conference*, Traverse City, MI, 2005.
[28] G.O. Ozgen, J. Kim, Direct identification and expansion of damping matrix for experimental-analytical hybrid modeling, *Journal and Sound Vibration* 308 (2007) 348–372.
[29] E.O. Brigham, *The Fast Fourier Transform and its Applications*, Prentice-Hall, Englewood Cliffs, NJ, 1988.
[30] R.W. Ramirez, *The FFT Fundamentals and Concepts*, Prentice-Hall, Englewood Cliffs, NJ, 1985.
[31] R.J. Allemang, R.W. Rost, D.L. Brown, Multiple input estimation of frequency response functions: excitation considerations, ASME Design and Production Engineering Technical Conference, *Dearborn, MI, ASME Paper Number 83-DET-73*, 1983.
[32] R.J. Allemang, *Vibrations: Analytical and Experimental Modal Analysis*, UC-SDRL-CN-20-263-662, Structural Dynamics Research Laboratory, University of Cincinnati, 1999.